18th IEEE International Conference on Advanced Thermal Processing of Semiconductors-RTP 2010

Comparison of Solid Phase Epi (SPE) Non-Melt to Liquid Phase Epi (LPE) Melt Laser Annealing for 22nm Node n+ USJ Formation

John Borland[1], Seiichi Shishiguchi[2], Norihiko Matsuzaka[2], Masami Hane[3], Masayasu Tanjyo[4], Peter Oesterlini[5] and Jeff Mayer[6]

[1]J.O.B. Technologies, Aiea, Hawaii
[2]Renesas Electronics Corp., Sagamihara, Japan
[3]Renesas Electronics America Inc., Albany, New York
[4]Nissin Ion Equipment Co. Ltd., Kyoto, Japan
[5]Jenoptik Innovavent GmbH, Gottingen, Germany
[6]Evans Analytical Group, East Windsor, New Jersey

***Abstract*- Arsenic, Phosphorus and Antimony dopants for n+ USJ formation was studied for junction quality comparing non-melt to melt laser annealing without and with BF_2 or In HALO structures. When junction leakage was high >2E-2A/cm^2 no reliable sheet resistance could be determined. We observed between 21nm to 70nm of liquid phase dopant diffusion with the melt process and dopant activation levels were lower than expected due to the very short annealing and cool-down quenching rates with laser annealing requiring longer dwell times. Also, cold implants and C co-implants with laser annealing resulted in very high junction leakage as did the additional of either a BF_2 or In HALO structure.**

INTRODUCTION

22nm node n+ USJ <10nm requires high quality junctions with high dopant activation, low junction leakage and tensile strain channel. Historically arsenic dopant has been used for n-type source drain extension (SDE) but at implant energies below 2keV, As activation is more difficult as reported by Noda et al. [1] requiring a deep 30keV Ge-PAI for 1keV As implant 1E15/cm^2 dose to maximize As dopant activation with msec laser annealing due to the shallower self-amorphous layer for As implants at low energies. Switching from As to Sb extension implantation, Kato et al. [2] showed slightly improve n+ dopant activation with Flash msec anneal (MSA). A comparison of As, Sb and P SDE dopant activation using spike anneal, fRTP Flash anneal and low temperature 650^{o}C SPE annealing was reported by Mineji et al. [3] and they showed P was best. With non-melt laser or Flash annealing the best P dopant activation seems to be limited to Pss<4E20/cm^3 [4]. Switching from non-melt laser to melt laser annealing Kennel et al. [5] showed that the highest n-type dopant activation can be realized with P (Pss=4E21/cm^3) over As (Ass=2E21/cm^3) and higher activation was observed with B (Bss=7E20/cm3) and In (Iss=5E19/cm^3). There are process integration issues with a melt process especially with high-k/metal gate first process flow but not so difficult with high-k/metal gate last. These current reported dopant activation values are higher than those reported back in 1960 by Trumbore [6] Sb=7E19/cm^3, B=6E20/cm^3, P=1.5E21/cm^3 and As=1.8E21/cm^3. Recently Kuhn et al. [7] also reported B-melt annealing flat chemical liquid phase diffusion (LPD) level of 2E21/cm^3 which was an electrical active Bss level of >5E20/cm^3 using laser melt processing. No recent laser melt data for As can be found in the literature but Kennel et al. [5] showed P-LPD chemical flat level of 5E21/cm^3 and active electrical Pss=1.8E21/cm^3. Jager et al. [8] also reported P chemical LPD flat level of 8E20/cm^3 (Pss electrical of 3E20/cm^3) for laser melt annealing when used for selective n+ emitter in solar cells. Other applications of laser melt annealing is for image sensors and IGBT [9, 10].

Another advantage of using P over As for n+ USJ is for gate overlap control. With MSA and minimal dopant diffusion As-dopant high tilt n+ SDE implantation is required to achieve the desired nMOS gate overlap [11-13]. However P tilted implantation is not necessary due to the significant amount of lateral straggle giving the required gate overlap at zero tilt implant [11]. There are very limited reports on HALO dopant activation with MSA and the data reported are not always in agreement showing differences between B, BF_2 and In HALO dopant activation levels due to differences in solid solubility limit with annealing temperature [3, 14]. Therefore this paper will report on our updated results comparing As, P & Sb for shallow n+ SDE and BF_2 or In for HALO using non-melt and melt laser annealing for Solid Phase Epitaxial (SPE) or Liquid Phase Epitaxial (LPE) regrowth for dopant activation annealing and junction leakage.

EXPERIMENTATION

The wafer experimental matrix split is shown in Fig.1. All the p-type 300mm wafers were provided by Renesas/Yamagata factory with approximately 2nm of surface oxide passivation. As, As_4, As_4-cold, P, P_4 and Sb n+ extension implants were compared at 1E15/cm^2 and 3E15/cm^2 doses for retained dose analysis, junction depth, dopant activation, residual implant damage and junction leakage. All of the monomer As and P implants were done at Renesas/Yamagata using a single wafer high current implanter while the As_4, As_4-cold, P_4 and Sb implants were

done at Nissin/Kyoto using their Claris molecular dopant implanter with cold-temperature option for the cold implant at -30°C. All the monomer and molecular As and P implants were done at 1keV equivalent while Sb was higher at 4keV due to implanter limitation with Sb-dopant. The C and C_{16} co-implants were also done by Nissin/Kyoto at 3keV 3E15/cm^2 carbon equivalent. Since in actual devices a p-type HALO dopant structure is present underneath the n+ SDE and the HALO dopant profile can dominate the n+/p junction leakage degradation we compared BF_2-HALO (20keV 3E13/cm^2 dose) to In-HALO (45keV 3E13/cm^2 dose) performed at Renesas/Yamagata using their medium current implanter.

		HALO Implantation	
		BF2-HALO	In-HALO
23-300mm p-type wafers	No HALO	20keV/3E13	45keV/3E13
•Control (n-type wafer)		#1(S6)	#2(S7)
•As (1keV/1E15)	#3(S1)	#4(S2)	#5(S3)
•As (1keV/3E15)	#6(S4)		
•As4 (1keV/1E15)	#9(S5)		
•P (1keV/1E15)	#10(S8)	#11(S9)	#12(S10)
•P (1keV/3E15)	#13(S11)		
•P4 (1keV/1E15)	#14(S15)	#15(S13)	#16(S14)
•P (1keV/3E15)+C(3keV/3E15)	#17(S18)		
•P4 (1keV/1E15)+C16(3keV/3E15)	#19(S19)	#20(S20)	#21(S21)
•P4 (1keV/3E15)+C16(3keV/3E15)	#22(S22)	#23(S23)	#24(S24)
•Sb (4keV/1E15)	#25(S25)		
•As4 (1keV/1E15) Cold/ Implant	#26(S12)		

Fig.1: Experimental matrix split conditions.

After all the implants were completed the wafers were sent to Applied Materials for non-melt laser annealing using the DSA process at 1250°C, 1300°C and 1350°C. The top half of the wafer received laser anneal line scans at 1250°C and 1300°C using 50% overlap so each region received 2 scans while the 1350°C laser anneal was just a single line scan so no overlap as shown in Fig.2. The wafers were then shipped to Jenoptik Innovavent Gmbh in Germany for laser melt annealing using the LAVA system with a laser field length of 8.26mm and 6um width. The wavelength was 515nm, pulse duration of 300nsec, pulse frequency of 10kHz and max power of 80watts. 26 separate areas were annealed on the notch half of the wafers in 2 columns and 13 rows as shown in Figs.3&4. The scan speed for column A was low and for column B high and the laser power energy density in row 1 was low ED (J/cm2) to high ED in row 13. Fig.4. illustration shows the various non-melt and melt laser annealing scan patterns for each 300mm wafer and the corresponding RsL wafer map image is shown in Fig.5 where the blue color is the no anneal regions and the yellow, orange and red color regions show the DSA laser diameter line scans in the lower half of the wafer and the double column line scans in the upper half of the wafer are from the LAVA laser melt annealer.

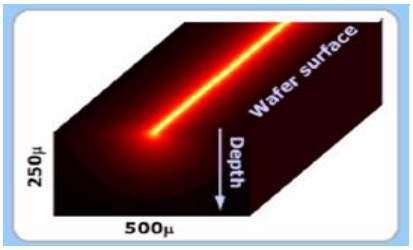

Temp	Y location
1250°C	-110
	-104.4
	-98.8
	-93.2
	-87.6
1300°C	-70
	-64.4
	-58.8
	-53.2
	-47.6
1350°C	-30

Fig.2: DSA laser anneal scan pattern.

Scan speed:
- column A: low
- column B: high

Energy density:

row	ED (J/cm²)
1	low
2	
3	
4	
5	
6	
7	
8	
9	
10	
11	
12	
13	high

Fig.3: Jenoptiks melt laser scan speed and power pattern.

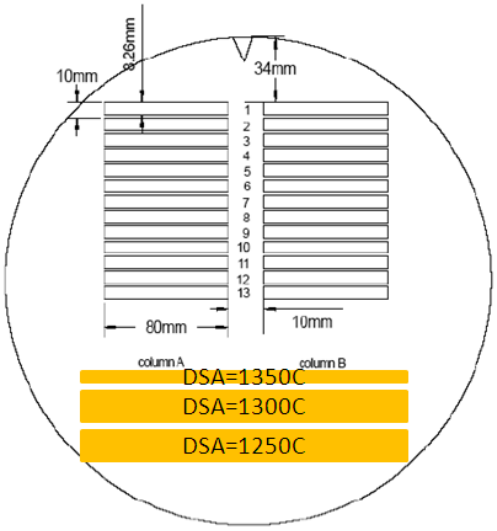

Fig.4: Laser annealing scan patterns for the non-melt and melt regions.

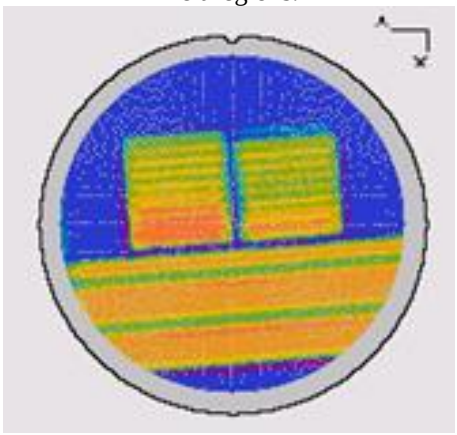

Fig.5: Actual RsL full wafer image showing the various laser annealing scan patterns.

RESULTS

Evans Analytical Group (EAG) measured the As & P dopant profiles using their special PCOR-SIMS technique. This allowed the determination of both the physical junction depth (Xj) and electrical junction depth Xj (Rs) profiles including surface oxide passivation thickness. Sheet resistance (Rs) and junction leakage (J_L) were measured by non-contact JPV (junction photo voltage) technique at Frontier Semiconductor using their RsL metrology system.

Plotting Rs versus Xj for the non-melt and melt dopant profile we then determined the electrical dopant activation level, dopant solid solubility as either Ass for arsenic, Pss for phosphorus or Sbss for antimony dopant species.

The PCOR-SIMS results for wafer #3 As=1keV 1E15/cm^2 dose is shown in Fig.6. The surface oxide thickness determined by SIMS is 1.7nm for the no anneal and 1300^{o}C annealed regions and was slightly thicker at 2.2nm for the laser melt region as mentioned earlier we expected 2.0nm of surface oxide. As-channeling was detected at 2E18/cm^3 and the retained dose was high at 110%. The abruptness improves from 1.9nm/decade as implanted to 1.6nm/decade with 1300^{o}C MSA. With the melt and resulting liquid phase diffusion (LPD), As abruptness degraded to 6.6nm/decade due to the 70nm of As-dopant LPD. The As dopant SIMS chemical flat level in the melt region was only 2E20/cm^3 due to the deep junction Xj=80.2nm resulting in dopant depletion. The P-dopant n+ USJ SIMS profiles for wafer#24 is shown in Fig.7. The sample was P_4+C_{16}+In-HALO for SiC+P n+ tensile strain-Si technology. The surface oxide was thicker than expected at 3.1nm for no anneal region, 2.8nm for 1300^{o}C anneal region and 3.2nm for the melt region. Note that a deep oxygen pile-up at 22nm depth was detected by SIMS which we believe represents the melt depth and also corresponds to the 21nm of P-dopant LPD movement caused by the melt depth. This oxygen pile-up was not detected for the As-dopant case possibly because the melt depth was much deeper resulting in the oxygen level to be below the lower SIMS detection limit. From the As-dopant LPD profile roll-off at 1E20/cm^3 we estimate the melt depth to be ~65nm but no oxygen marker can be detected. The P-dopant flat level for the 1300^{o}C anneal is 2E21/cm^3 as clearly shown in Fig.7 and drops to 1.2E21/cm^3 for the melt anneal region. This is much higher than the 8E20/cm^3 P-dopant LPD flat level reported by Jager for laser melt solar cells with shallower LPD and 3E20/cm^3 for deeper LPD [8] but very similar to the 1.5E21/cm^3 LPD flat level reported by Kennel [5]. The P-dopant abruptness for the no anneal region is 2.3nm/decade, 2.1nm/decade for the 1300^{o}C anneal region and 2.9nm/decade for the melt anneal region. Also the difference in the melt depth and LPD (22nm versus 65nm) may be due to the presence of the C implant or differences in amorphous layer depth requiring further study.

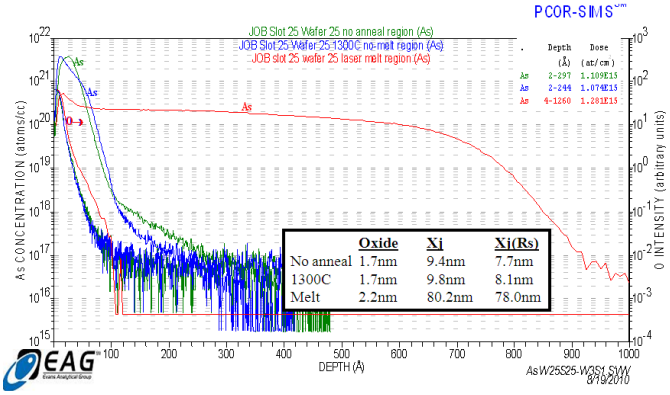

Fig.6: Wafer#3 As n+ USJ SIMS depth profile.

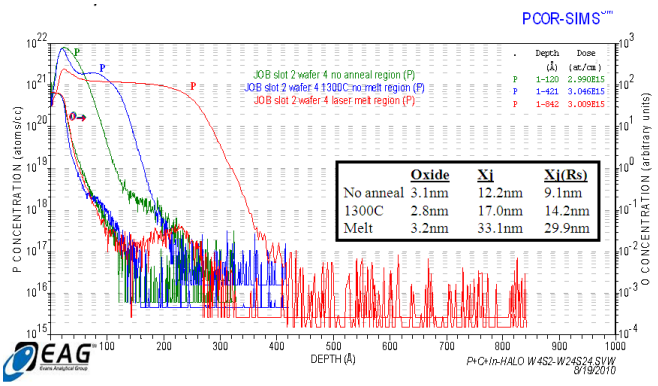

Fig.7: Wafer#24 P_4+C_{16}+In-HALO SIMS depth profile.

N+ USJ without HALO

The full wafer RsL image showing the various laser annealing line scanning pattern for Rs and J_L is shown in Fig.8. Diameter line scan data were taken as shown with the blue arrow going from quadrant 3 (Q3) to 1 (Q1) and red arrow going from quadrant 4 (Q4) to 2 (Q2) as shown in Fig.9 in order to compare melt laser column A to B as described in Figs.3&4. The RsL junction leakage (J_L) results for n+ USJ without HALO are shown in Fig. 10 and the corresponding sheet resistance (Rs) are shown in Fig. 11. The J_L values are generally below 1E-5A/cm^2 for the As, P and Sb n+ USJ except for the As-cold implant and one of the C co-implant case where the J_L values increased by over 3 orders of magnitude to above the upper leakage detection limit of >2E-2A/cm^2. The very leaky junctions explains the low measured Rs of 100-600 ohms/sq for the As-cold implants compared to 4000-7000 ohms/sq for the good leakage As junctions. High levels of C has been reported to degrade junction leakage but the As-cold implant was expected to improve not degrade junction leakage so this result is interesting requiring further study. Also the improved J_L for C implant with higher P dose of 3E15/cm^2 is similar to that reported by Borland last year [4].

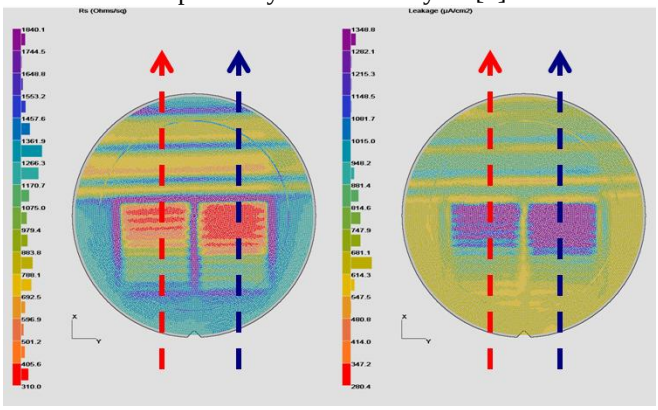

Fig.8: JPV full wafer image showing the various laser line scan patterns detected by Rs (left) and JL (right) analysis.

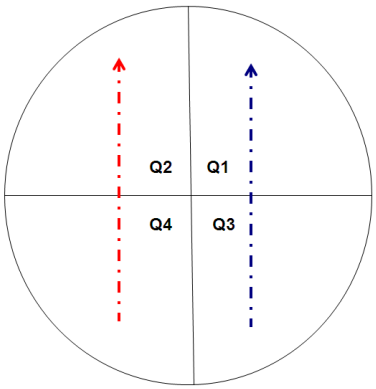

Fig.9: JPV diameter line scan direction to measure Q1 and Q3 with blue arrow scan direction and Q2 and Q4 with red arrow scan direction.

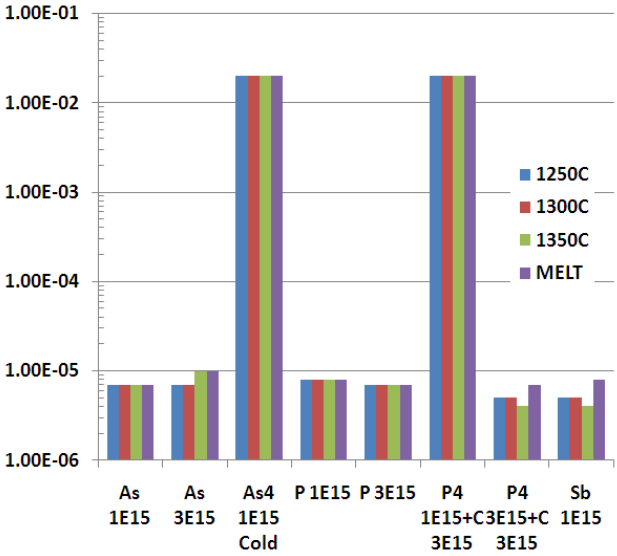

Fig.10: RsL junction leakage results for As, P & Sb n+ USJ without HALO.

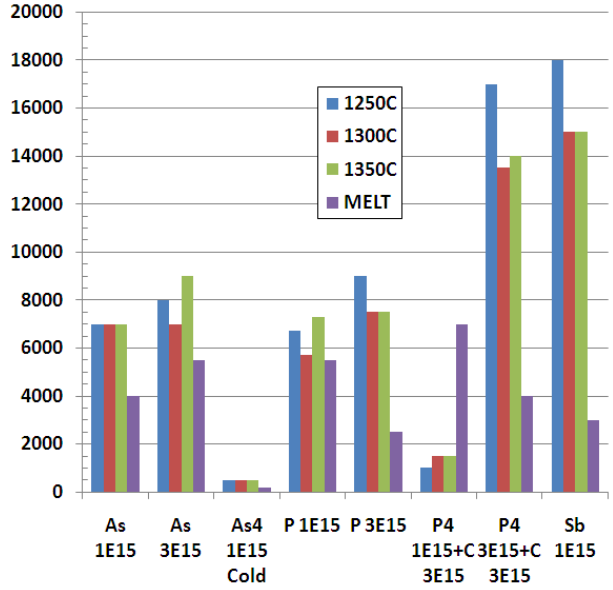

Fig.11: RsL sheet resistance results for As, P & Sb n+ USJ without HALO.

The detailed Rs and J_L full wafer image mapping for As=1keV/1E15 is shown in Fig. 12 and the diameter RsL line scans from Q3 to Q1 and from Q4 to Q2 is shown in Fig.13. The Rs line scan values for the DSA 1250°C, 1300°C and 1350°C annealed regions are the same for the blue Q3 to Q1 and red Q4 to Q2 scans in Fig.13 while the LAVA melt laser annealed Rs values are lower with the blue low scan speed column A at higher power. However, we expected much lower Rs values by about 7x for example 1000 ohms/sq rather than 7000 ohms/sq for 1300°C to realize an As dopant activation solid solubility level of Ass>1.3E20/cm^3 rather than the measured low Ass level of 3E19/cm^3. The J_L values are all good in the mid-E-6A/cm^2 level. Even the laser melt Rs is high (4000 ohms/sq) but Xj (Rs) from SIMS in Fig.6 is 78.0nm for a very low Ass<8E18/cm^3. These lower Ass levels suggest the laser annealing conditions require further optimization, poor dopant activation for laser annealing was reported by Borland et al. [15] because the annealing time (dwell time) was too short or cooling/quenching rate too fast preventing complete epitaxial crystal alignment with remaining partial amorphous region. Kato et al. also reported similar effects for Flash MSA [16]. The high leakage As-cold implant RsL wafer map is shown in Fig. 14 and note that the Rs wafer map on the left side looks OK showing all the various laser annealing scan pattern but the right side J_L wafer map only detects 2 laser melt scan pattern region low scan with 2 highest power levels and nothing else because of the high leakage level above the upper detection limit of >2E-2A/cm^2. The J_L diameter line scans are shown in Fig.15 and the 2 detected laser melt region J_L is improved 20-50x to <1E-3A/cm^2 with an Rs value 650-750 ohms/sq. The P=1keV/1E15 condition results are shown in Fig. 16 for RsL wafer map and Fig. 17 for RsL diameter line scans. The J_L values are good in the 1E-5A/cm^2 range with the Rs values are higher than expected, 6750 ohms/sq for 1250°C, 5750 ohms/sq for 1300°C, 7250 ohms/sq for 1350°C and 5500 ohms/sq for melt. The RsL wafer map and diameter line scan for the added C co-implant results are shown in Figs. 18 & 19. C degrades J_L to >2E-2A/cm^2 so the Rs values are not reliable. When the P dose is increased to 3E15/cm^2 equal to the C dose then leakage dramatically improves to mid-E-6A/cm^2 range as shown in Figs. 20 & 21 but now the Rs values were very high at >14,000 ohms/sq for DSA and 4000 ohms/sq for melt. Results for Sb n+ USJ are shown in Figs. 22 & 23 showing good low leakage (mid-E-6A/cm^2) but again the Rs seems much higher than expected suggesting poor dopant activation >15,000 ohms/sq for non-melt laser and 3000 ohms/sq for melt laser.

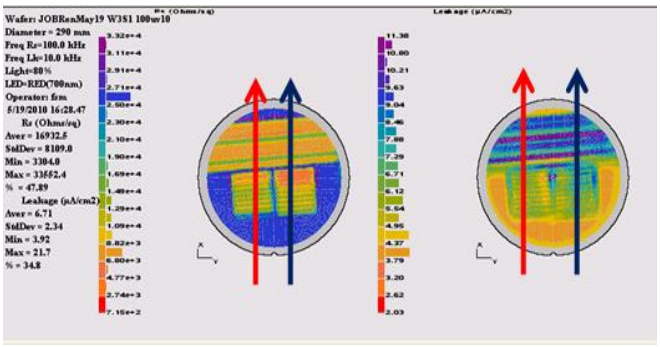

Fig.12: Rs and J_L wafer map for As=1keV/1E15.

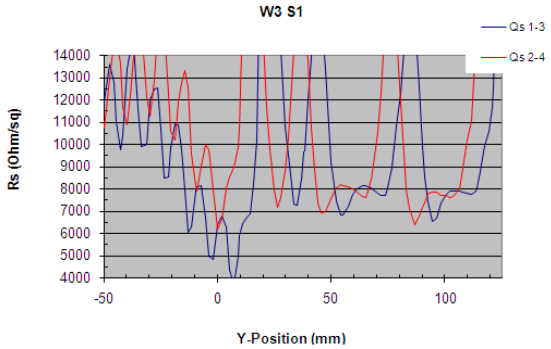

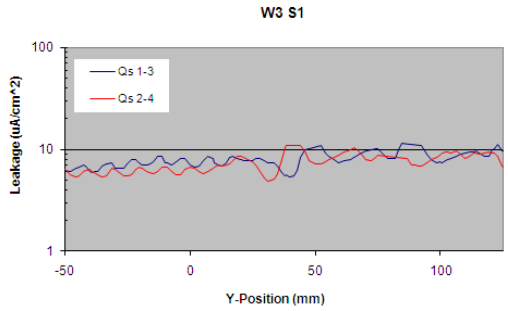

Fig.13: Rs and J_L line scans of Q1-3 ad Q2-4 for As=1keV/1E15.

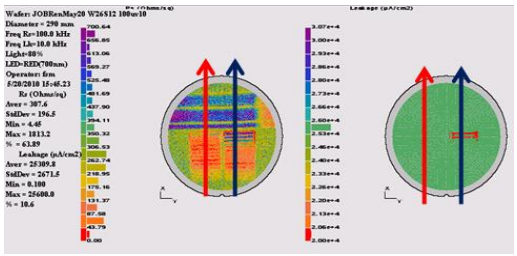

Fig.14: Rs and J_L wafer map for As-cold implant 1keV/1E15.

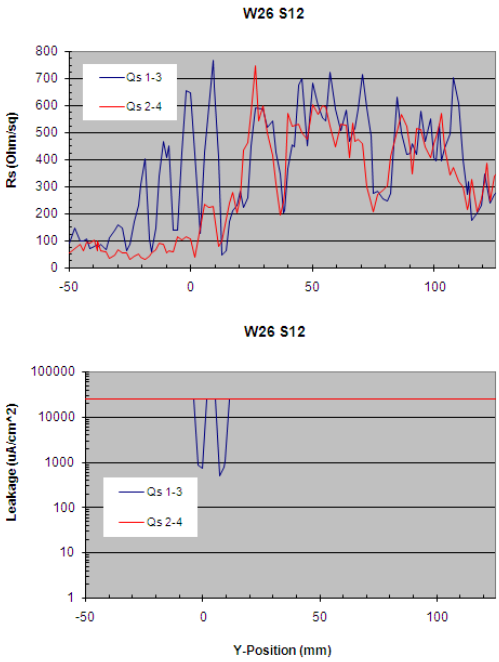

Fig.15: Rs and J_L line scans of Q1-3 ad Q2-4 for As cold implant.

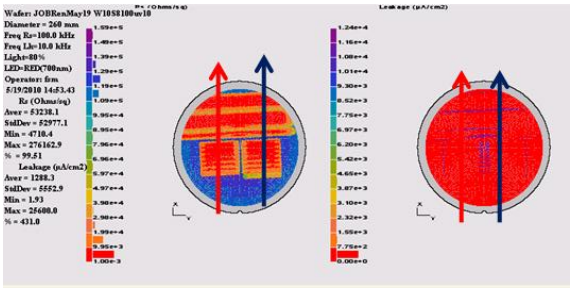

Fig.16: Rs and J_L wafer map for P=1keV/1E15.

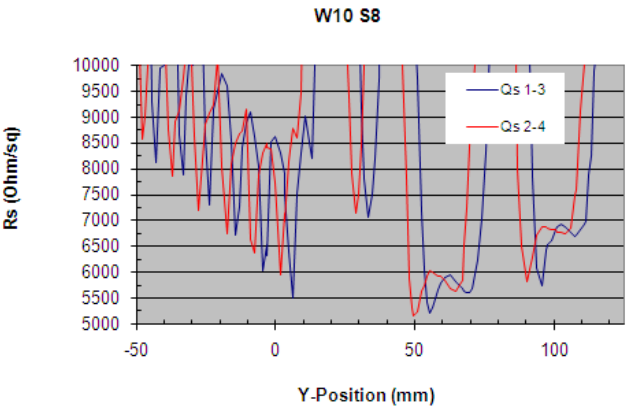

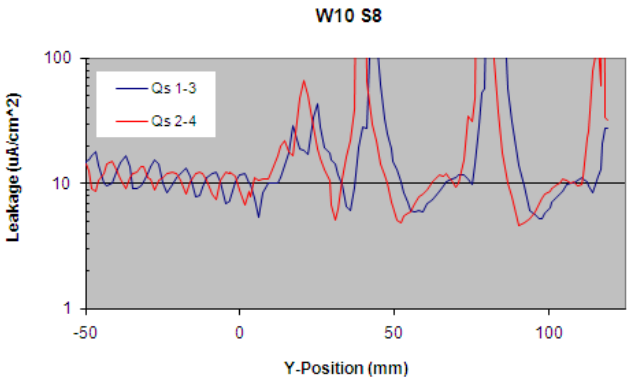

Fig.17: Rs and J_L line scans of Q1-3 ad Q2-4 for P=1keV/1E15.

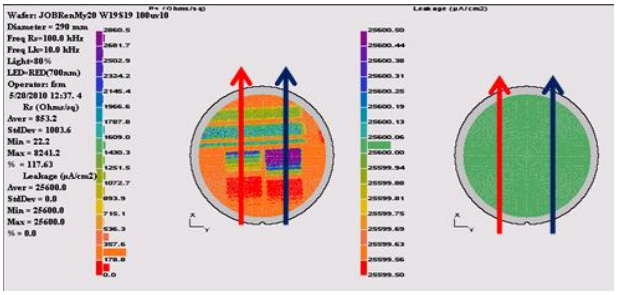

Fig.18: Rs and J_L wafer map for P_4=1keV/1E15 + C_{16}=3keV/3E15.

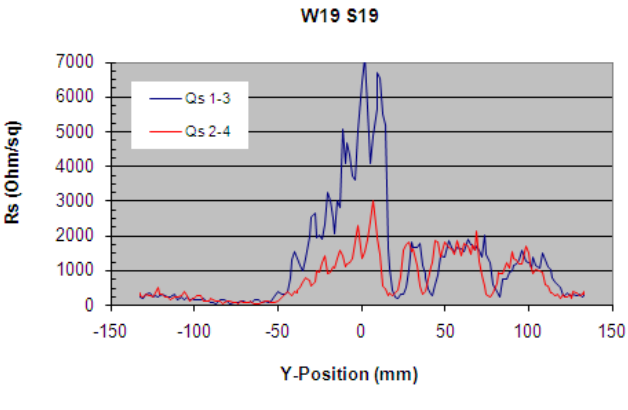

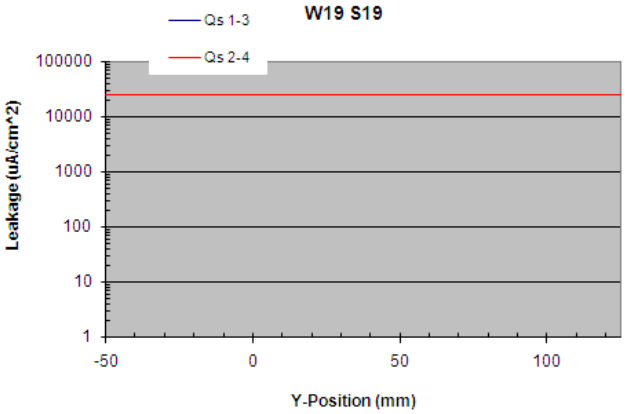

Fig.19: Rs and J_L line scans of Q1-3 ad Q2-4 for P_4=1keV/1E15 + C_{16}=3keV/3E15.

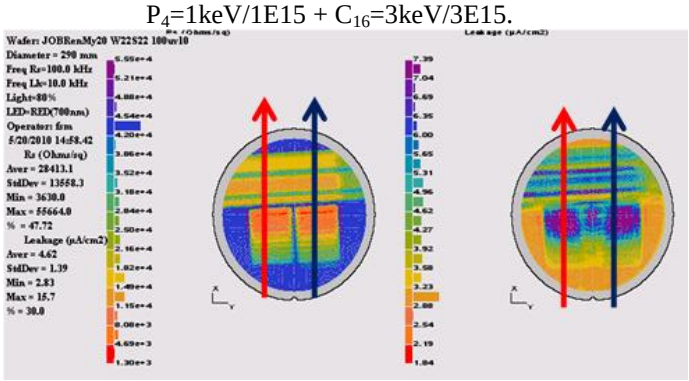

Fig.20: Rs and J_L wafer map for P_4=1keV/3E15 + C_{16}=3keV/3E15.

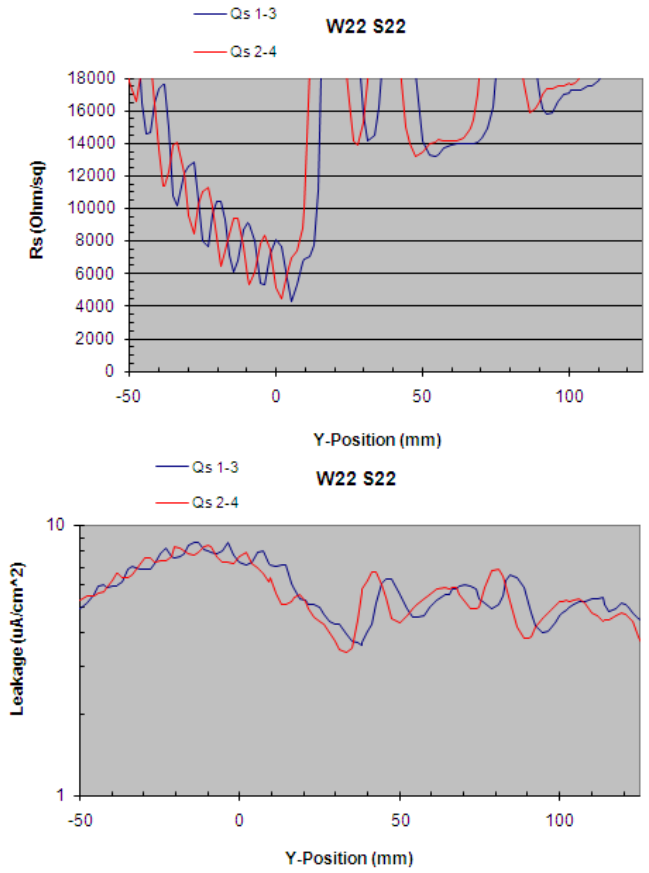

Fig.21: Rs and J_L line scans of Q1-3 ad Q2-4 for P_4=1keV/3E15 + C_{16}=3keV/3E15.

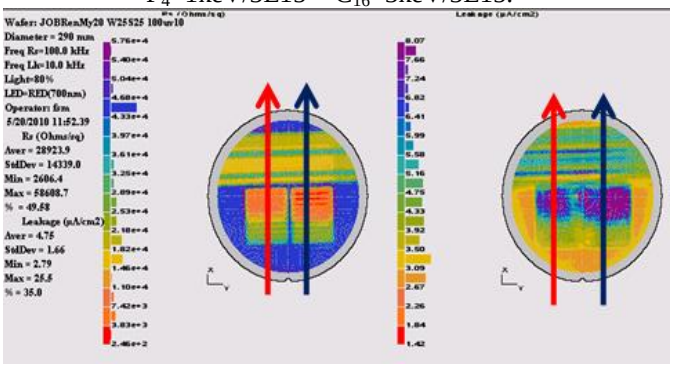

Fig.22: Rs and J_L wafer map for Sb=1keV/1E15.

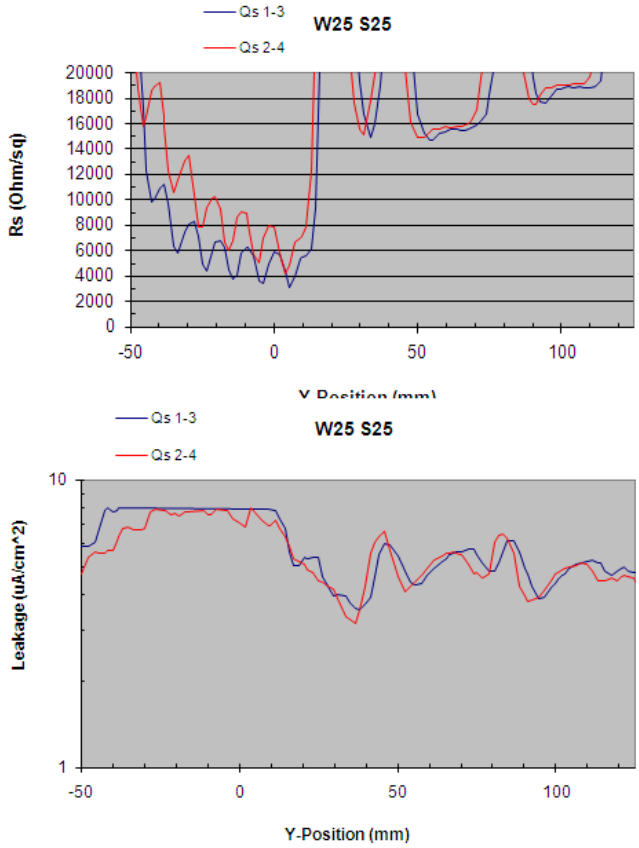

Fig.23: Rs and J_L line scans of Q1-3 ad Q2-4 for Sb=1keV/1E15.

N+ USJ with HALO

The J_L results with BF_2 or In HALOs are shown in Fig.24 and Rs results in Fig.25. With the HALO structure all the n+ junctions leakage values were >2E-2A/cm^2 except for the P+In-HALO which showed lower leakage by >100x with MSA temperature >1300^{o}C suggesting In dopant activation may be different at higher MSA temperatures as reported elsewhere by Borland [17]. The detailed RsL wafer maps and line scans for this P+In wafer are shown in Figs. 26 & 27. The J_L wafer map in Fig. 26 could not detect the 1250^{o}C DSA laser scan region which was very leaky >2E-2A/cm^2 as shown in Fig.27 with no reliable Rs value which varies from 1000-9000 ohms/sq. With the 1300^{o}C anneal J_L improves to 5E-5A/cm^2 and Rs=2700 ohms/sq. (Pss=5E19/cm^3), at 1350^{o}C J_L=1E-4A/cm^2 and Rs=2200 ohms/sq. and melt anneal J_L=1.7E-4A/cm^2 and Rs=<1000 ohms/sq. (Pss=4E19/cm^3).

.

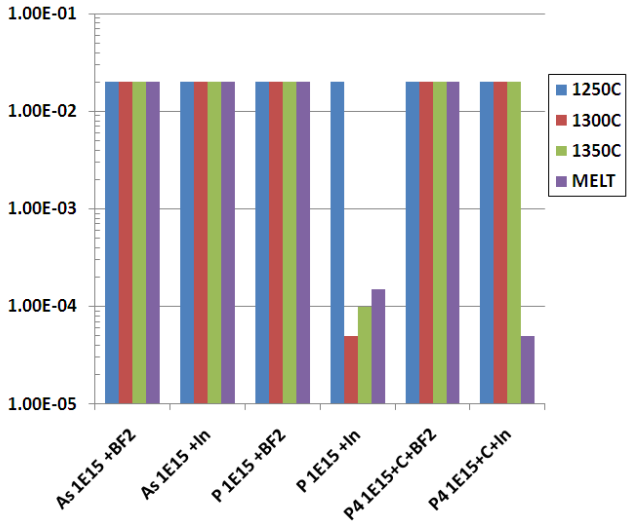

Fig.24: RsL junction leakage results for As & P n+ USJ with BF_2 and In HALOs.

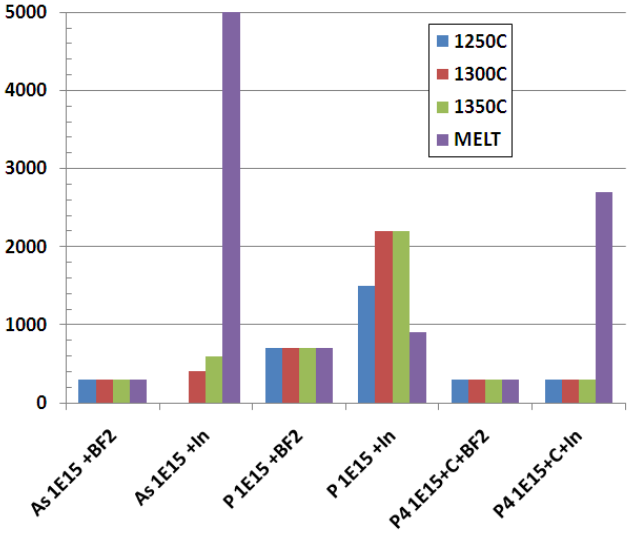

Fig.25: RsL sheet resistance results for As & P n+ USJ with BF_2 and In HALOs.

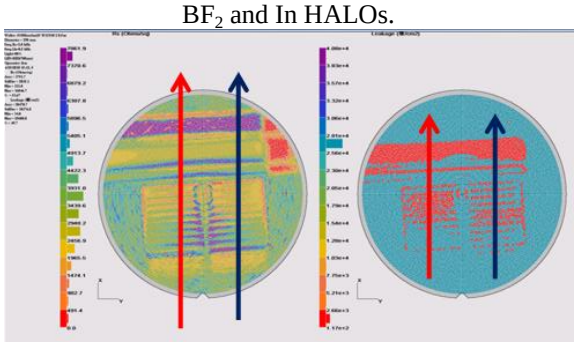

Fig.26: Rs and J_L wafer map for P=1keV/1E15 + In-HALO.

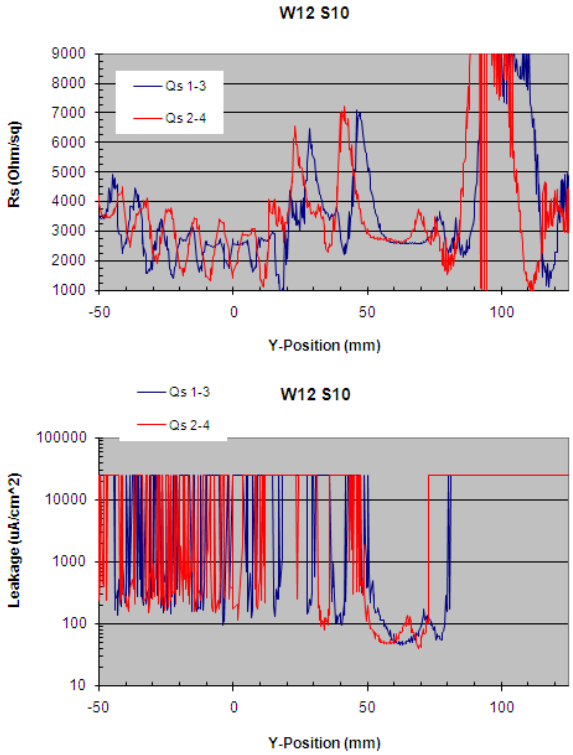

Fig.27: Rs and J_L line scans of Q1-3 ad Q2-4 for P=1keV/1E15 + In-HALO.

SUMMARY

As, P and Sb dopants for n+ SDE was investigated using non-melt laser annealing via solid phase epitaxial regrowth and compared to laser melt annealing via liquid phase epitaxial regrowth. The measured sheet resistance values were significantly higher than we expected resulting in dopant activation levels in the high E18/cm^3 to low E19/cm^3 rather than the expected E20 to E21/cm^3 level expected with laser non-melt and melt annealing suggesting poor SPE and LPE dopant activation. When junction leakage was high the Rs value was not reliable. Both cold implant and C co-implants with laser annealing resulted in very high junction leakage. Also the addition of the BF_2 or In HALO resulted in very high leakage requiring further process optimization. PCOR-SIMS showed nearly 100% retained dose and detected oxygen pile-up at the melt liquid phase interface which corresponded to the liquid phase diffusion depth.

ACKNOWLEDGMENTS

The authors are grateful to Frontier Semiconductor for RsL sheet resistance and junction leakage measurements especially to Ann Koo, Michael Current and Iad Mirshad for their support. Also to Jeremy Zelenko of Applied Materials for support with the DSA laser anneals.

REFERENCES

1] T. Noda et al., "Analysis of As, P Diffusion and Defect Evolution During Sub-millisecond Non-melt Laser Annealing

Based on an Atomistic Kinetic Monte Carlo Approach", IEDM 2007, section 36.5.1, p.955.
2] S. Kato, T. Aoyama, T. Onizawa, Y. Nara and Y. Ohji, "Study of Ultra-Shallow Junctions Formed by Flash Lamp Annealing to Reveal Dopant Activation Phenomenon", IWJT 2007, paper S8-5, p.143.
3] A. Mineji, J. Borland, S. Shishiguchi, M. Hane, M. Tanjyo and T. Nagayama, "Molecular Dopants and High Mass Dopants For HALO and Extension Implantation", IWJT 2007, paper S4-8, p.73.
4] J. Borland et al., "22nm node n+ SiC Stressor Using Deep PAI+C_7H_7+P_4 with Laser Annealing", IEEE/RTP 2009, p.59.
5] H. Kennel et al., "Kinetics of Shallow Junction Formation: Physical Mechanisms", IEEE/RTP 2006, paper 13, p.85.
6] F. Trumbore, Bell System Tech. J., vol. 39, p. 205, 1960.
7] K. Kuhn, M. Liu and H. Kennel, "Technology Options for 22nm and Beyond", IWJT 2010, paper K2, p.7.
8] U. Jager, S. Mack, A. Kimmerle, A. Wolf and R. Preu, "Influence of Doping Profile of Highly Doped Regions for Selective Emitter Solar Cell", 35th IEEE PVSC 2010, paper 806, to be published.
9] K. Huet et al., "Activation of Ion Implanted Si for Backside Processing by Ultra-fast Laser Thermal Annealing: Energy Homogeneity and Micro-scale Sheet Resistance", IEEE/RTP 2009, p.105.
10] Y. Arai, T. Matsuda, T. Kudo, K. Sanna, H. Schmidt and P. Oesterlin, "Backside Activation Technique of Power Device IGBTs by a Microsecond-Pulsed Green Laser", IEEE/RTP 2009, p.117.
11] J. Borland and V. Moroz, "Implantation and Annealing Options for 65nm Node SDE Formation", Semiconductor International, April 2003, p.72.
12] C. Ortolland et al., "Laser Annealed Junctions with Advanced CMOS Gate Stacks for 32nm Node: Perspectives on Device Performance and Manufacturability", VLSI Sym 2008, paper 19.1, p.186.
13] Ootsuka et al., "Ultralow Thermal Budget CMOS Process Using Flash Lamp Annealing For 45nm Metal/High-k FET", IEEE Transaction Electron Devices, vol.55, no.4, April 2008, p. 1042.
14] J. Borland and H. Kiyama, "Comparison of B, BF_2 & $B_{18}H_{22}$ Extension and BF_2, $B_{18}H_{22}$ & In HALO Implantation for 32nm Node Using Various Diffusion-less Annealing Techniques", IIT-2008, p.63.
15] J. Borland et al., "45nm Node p+ USJ Formation with High Dopant Activation and Low Damage", IWJT-2006, p.4.
16] S. Kato, Y. Nara, T. Aoyama, T. Onizawa and Y. Ohji, "Dopant Activation Phenomenon by Flash Lamp Annealing", ECS May 2008, ECS Transactions, vol.13, no.1, p.45, 2008.
17] J. Borland et al., "22nm node p+ USJ Defect Analysis with Various PAI and HALO Structures Using Laser Annealing", IEEE/RTP 2010, these proceedings.